Asian Journal of Chemistry; Vol. 30, No. 12 (2018), 2671-2676

ASIAN JOURNAL OF CHEMISTRY

https://doi.org/10.14233/ajchem.2018.21543

Nanoscale Phenomena During Crystal Growth of $Ca_xCd_{1-x}CO_3$ Solid Solution at Calcite Surface Exposed to Cadmium Bearing Aqueous Solution

WENLEI WANG[1,*], TIANLI YANG[1], JIAO SHI[2], REN HE[1], HAN HUANG[2], YUNCHU HU[1] and LICHAOWU[3]

[1]College of Science, Central South University of Forestry and Technology, Changsha 410004, Hunan Province, P.R. China
[2]Hunan Key Laboratory for Super-microstructure and Ultrafast Process, Central South University, Changsha 410083, Hunan Province, P.R. China
[3]Key Laboratory of Cultivation and Protection for Non-Wood Forest Trees, Ministry of Education, Central South University of Forestry and Technology, Changsha 410004, Hunan Province, P.R. China

*Corresponding author: E-mail: wenlei_wang@hotmail.com

Received: 27 June 2018; *Accepted*: 1 September 2018; *Published online*: 31 October 2018; AJC-19130

The crystal growth of $Ca_xCd_{1-x}CO_3$ solid solution play an important role in understanding the transformation relationship of the calcite surface exposed to cadmium-bearing aqueous solution. *in situ* AFM measurements were used to perform the real-time tracking of surface precipitates that are generated on the surface of calcite single crystals reacted with Cd^{2+} solution. As evidenced by changes in the height, shape and growth behaviour, two-dimensional epitaxial island was detected to form and grow on the surfaces. These detections of the generated crystals by SEM, EDS and TEM have demonstrated the formation of an epitaxial $Ca_xCd_{1-x}CO_3$ solid solution. The epitaxial solid solution within nanometers was first rich in caelement and the content of cadmium increased with the distance from the original calcite surface, culminating almost pure $CdCO_3$ in the topmost region. A low-cadmium solid solution with thermodynamic instability could be transformed into a cadmium-rich solid solution and form continuous solid solution in the process of maturation. This study aims to provide a better understanding of nanoscale features of the surface precipitation process at calcite surface in the presence of cadmium.

Keywords: Crystal growth, Solid solution, $Ca_xCd_{1-x}CO_3$, Calcite.

INTRODUCTION

Cadmium has been recognized as one of the most concerning heavy metal pollutants because of its strong biological accumulation and persistent toxicity and has been of particular concern due to its common source of pollution, serious pollution status and nonnegligible health risks [1-4]. Immobilization of cadmium will always occur in the presence of calcite with a rhombohedral structure by the formation of an isomorphic phase [5-9]. The natural self-purification of cadmium pollution by natural marble and shell powder was also proposed [10].

The removal of cadmium by calcite has become an important research topic in the study of cadmium pollution control in rivers, lakes and other water bodies [11,12]. The precipitation mechanism for the interaction of the calcite surface exposed to Cd-bearing aqueous solutions will play important roles in natural and industrial processes of Cd^{2+} uptake by calcite. However, this mechanism of crystal growth of $Ca_xCd_{1-x}CO_3$ solid in aqueous solution remains largely unexplored. In this paper, the crystal growth of $Ca_xCd_{1-x}CO_3$ solid solution was carried out by exposing calcite surface to Cd-bearing aqueous solutions at 283.1 K. To prove the formation of a solid solution and identify the type of solid solution, the nucleation process of $Ca_xCd_{1-x}CO_3$ solid solution was further investigated using CO_2 diffusion technology to aqueous solutions containing 0.05 M Cd^{2+} and 0.05 M Ca^{2+}. Atomic force microscope (AFM) and scanning electron microscope (SEM) were employed as the primary technique for the investigation of morphology of the microstructure and heteroepitaxial growth of generated crystal at the calcite-water interface. High-resolution transmission electron microscopy (HRTEM) measurements were used to perform tracking of crystal growth of $Ca_xCd_{1-x}CO_3$ solid solution and analyze the composition, lattice distribution and element distribution of the generated crystal.

EXPERIMENTAL

Fresh calcite substrates were prepared from optically clear calcite crystals obtained from GuiZhou Province by cleaving

with a sharp knife along ($10\bar{1}4$) cleavage plane with dimensions of approximately 10 mm × 12 mm × 1.5 mm. The obtained specimens were then placed in deionized water with ultrasonic treatment for 20 min in order to clean the crystal surface. Aqueous solutions of Ca^{2+} and Cd^{2+} were prepared from high-purity $CdCl_2$ and $CaCl_2$ (> 99 %, Sinopharm Chemical Reagent Co., Ltd.) dissolved in deionized water ($S < 1.5 \times 10^{-4}$ S m^{-1}) and measured by an inductively coupled plasma optical emission spectrometer (ICP-OES, 5300DV, Perkin-Elmer, USA). The precipitationexperiments were carried out in a thermostat (Lauda E219, Germany) with temperature stability up to ± 0.01 K at 283.1 K.

Experimental procedure of exposing calcite surface to cadmium bearing aqueous solutions: *in situ* Atomic force microscope (AFM) (Bruker, Dimension Icon) experiments were carried out in static conditions by first contacting the calcite surfaces with 3.5 mL deionized water for 0.5 h and transferred into a reagent vessel that was fully filled with N_2 with a pair of antistatic plastic forceps and then by introduction of a certain volume of stock solution to obtain the certain initial Cd^{2+} concentration. Each sample was reacted for a certain time after, which each calcite crystal was removed from solution and dried immediately with pressurized N_2 (g) for analysis. AFM images were then taken every few minutes in contact mode using the dimension icon atomic force microscope. The Au-coated silicon nitride probes (Brucker, NP-10, nominal force constant of 0.12 Nm^{-1}) were employed for AFM imaging. To reduce the probe's disturbance to the mineral surface, the external load was usually smaller than 15 nN. The scanning frequency ranges from 165.7 to 165.8 Hz with 512 sampling points per scan line. SEM images were recorded using a Philips-PEI model Quanta 200. The chemical elements of new epitaxial phase were determined by the EDS analysis.

Nucleation process of $Ca_xCd_{1-x}CO_3$ solid solution: Furthermore, 10 mL of aqueous solution mixed with 0.05 M Cd^{2+} and 0.05 M Ca^{2+} was first transferred to a watch glass. The above watch glass was placed in a sealed reactor. Then, a beaker containing ammonium bicarbonate was placed around the watch glass for releasing CO_2 to provide a source of CO_3^{2-} for the formation of a solid solution. Samples were taken over time and analyzed by TEM to perform real-time tracking of nucleation process of the solid solution.

RESULTS AND DISCUSSION

Exposing calcite surface to cadmium-bearing aqueous solutions: Fig. 1 presents time-sequential images of calcite surface in contact with 0.05 mM Cd^{2+}, illustrated the progressive expansion of islands with time. After exposure to the above solution, the epitaxial phase visibly formed on calcite surface and exhibited a characteristic two-dimensional structure (Fig. 1b-c). The epitaxial phase possessed crystal nuclei for heteroepitaxial growth of the precipitates and provides a considerable number of active sites for further precipitation of Ca^{2+} or Cd^{2+}. Surface precipitates obtained in 360 min experiments showed similar features to those observed for crystals reacted for 15 and 30 min that is, islands elongated along the [42-1] and [010] directions (Fig. 1d). This type of precipitate will therefore be referred to as epitaxial islands. AFM observations revealed a two-stage process in the nucleation of surface precipitates in agreement with reports in the literature [13-17]. A precursor phase was observed to initially form on the surface and subsequently undergo an epitaxy-mediated phase transformation to epitaxial phase and a more stable crystalline phase.

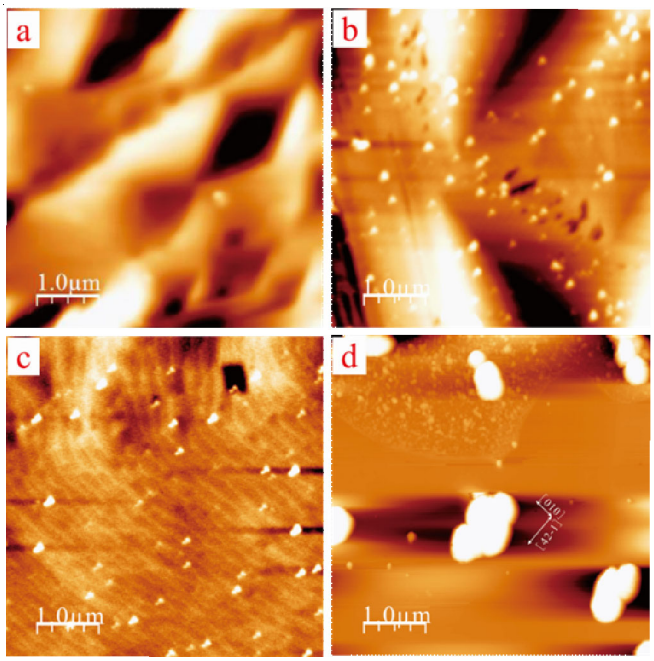

Fig. 1. Sequences of AFM topography (1000 nm × 1000 nm) of calcite ($10\bar{1}4$) surface in contact with Cd-bearing aqueous solutions. Images were taken at t = 0 min (a), t = 15 min (b), t = 30 min (c), t = 360 min (d)

As shown in Fig.2a, the surface precipitate was consistent with the island morphology measured *in situ* AFM experiments. The obvious step of epitaxial phase indicates that the nucleation and growth of the islands proceeded layer by layer as well as by a step advance. Layer-by-layer growth was also observed in other investigations, for instance, Cubillas and Higgins [18] observed the formation of "single-layer and multilayer islands" on calcite surfaces exposed to aqueous solutions containing bivalent metal ions. According to crystal nucleation theory of surface reactions, the most likely location of nucleation should be the position with the most favourable Gibbs free energy of formation, or a position with more nuclear activity sites. A kink site is one such site and leading edge of the steps is the other such site. Once a particle is deposited onto the crystal surface, the other particles are rapidly deposited to the leading edge of step, forming the entire particle layer. The first particle deposited on crystal surface can be considered to be a core of two-dimensional growth, which begins a new crystal layer exactly as a three-dimensional growth. The expansion of monolayer etch pits was observed, indicating the dissolution of calcite surface releasing CO_3^{2-} and providing CO_3^{2-} to participate in the formation of solid solution (Fig. 2b).

The time for calcite surface in contact with 0.05 M Cd^{2+} was extended to a long enough time for about half a year to estimate whether cadmium ion is infiltrated into calcite lattice. As observed in Fig. 3a-b, the preferred growth of epitaxial crystal

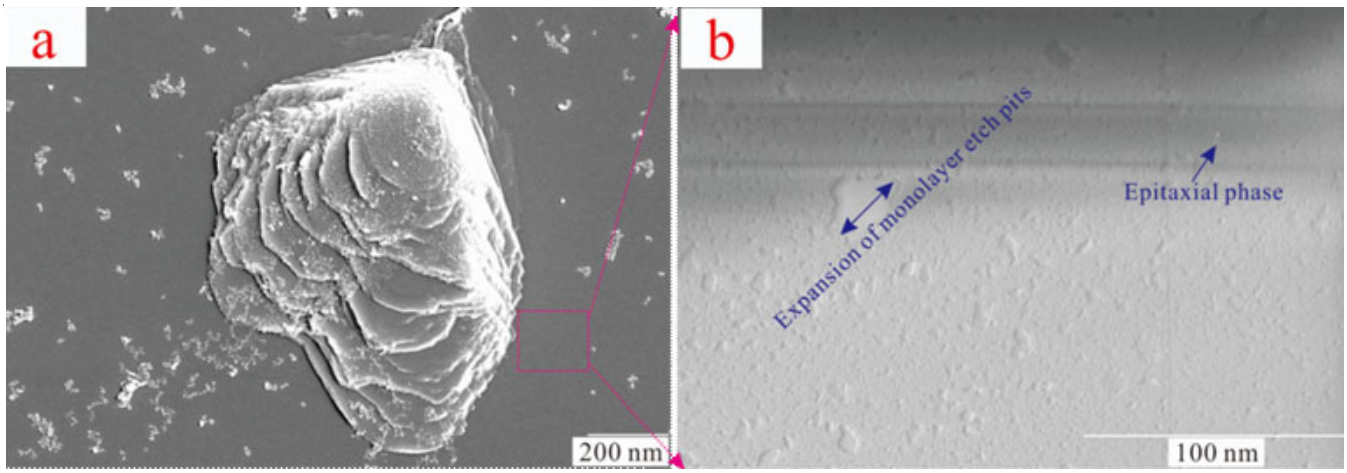

Fig. 2. SEM images of calcite $(10\bar{1}4)$ surface in contact with Cd-bearing aqueous solutions. Images were taken at t = 360 min

grew a long a same specific crystallographic direction. The epitaxial crystal was clearly commensurate with the calcite crystal substrate and there was no evidence of inclusions or the secondary phases. As can be seen in Fig. 3c-d, the epitaxial crystal could grow to approximately 3 μm in length. Additionally, many corrosion pits were observed on the calcite crystal surface. To determine the composition of generated epitaxial crystals, EDS measurement was carried out along the extension of the newly generated crystals. The composition of measured samples of epitaxial crystals at a distance of 100 nm, 1.2 μm and 2 μm from the origin calcite surface (labeled separately as points 2, 3 and 4 in Fig. 3a) were $Ca_{0.9217}Cd_{0.0683}CO_3$, $Ca_{0.6873}Cd_{0.3127}CO_3$ and $Ca_{0.3155}Cd_{0.6845}CO_3$, respectively. The composition changes of these solid solution crystals collectively confirmed the characteristics of oriented growth of solid solution along the epitaxial direction on the investigated time scale. With growth, the content of

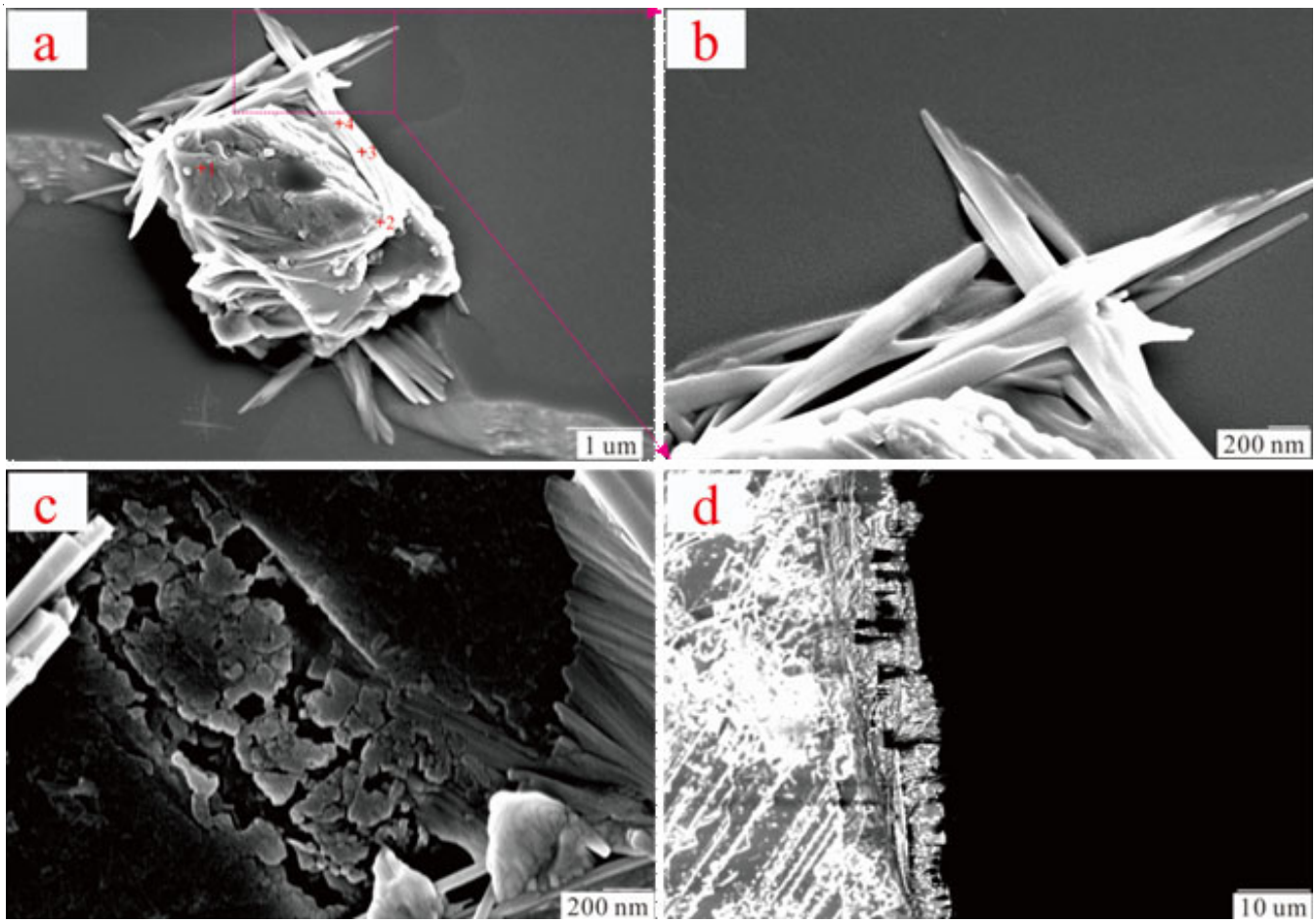

Fig. 3. FE-SEM images of an oriented aggregation of the $Ca_xCd_{1-x}CO_3$ solid solution after a one-year reaction at 283.15 K. (a) and (d) provide the details. (c) shows corrosion pits observed on the surface of calcite crystals, indicating the dissolution of the calcite surface with releasing CO_3^{2-}. (d) Cross section of the corrosion pits

cadmium in the solid solution gradually increased. Ultimately, the generated crystals could form otavite by oriented growth.

Nucleation process of $Ca_xCd_{1-x}CO_3$ solid solution: Time-sequential TEM measurements were carried out in air following a 360 min nucleation period in inert atmosphere with 0.05 M Cd^{2+} and 0.05 M Ca^{2+} to understand the early crystallization behaviour of $Ca_xCd_{1-x}CO_3$ crystal with the results shown in Fig. 4. Although the growth conditions were different, the TEM images suggest that the crystal islands observed in the AFM experiments could be generally free of dislocations with a fully epitaxial structure. At a reaction time of 5 min, an amorphous precipitate first appeared in confinement under conditions. As shown in Fig. 4b, almost all these amorphous particles were singly dispersed and sparsely distributed individual nanoparticles of diameter 10-15 nm. The amorphous particles present after 30 min had all aggregated, but they were almost exclusively isolated particles after 60 min. This strongly suggests that the degree of aggregation plays a key role in defining. The formation of a nucleus of more stable polymorph rapidly destabilizes the original population of metastable particles.

The crystallization process based on aggregation is always accompanied by reorientation and reconstruction. HRTEM and EDS measurements were performed to analyze the composition, lattice distribution and element distribution of the generated crystal with results listed in Table-1. The composition of the solid solution can be obtained by analyzing the EDS results. The solid solution generated was $Ca_{0.9659}Cd_{0.0341}CO_3$, $Ca_{0.3289}Cd_{0.6710}CO_3$, $Ca_{0.1461}Cd_{0.8538}CO_3$ and $Ca_{0.0423}Cd_{0.9576}CO_3$ for the reaction time of 15 , 45, 60 and 360 min, respectively. With increasing reaction time, the content of Cd^{2+} in solid solution increased from 0.0341 to 0.9576 of cadmium atomic percent. However, the rate of increase decreased. This result indicated that Cd^{2+} could continually permeate through the crystal lattice while replacing Ca^{2+} in the formation of solid solution. The increase in Cd^{2+} content in solid solution hindered the penetration of Cd^{2+} into the solid solution crystal lattice to some extent.

TABLE-1
EDS RESULTS OF THE GENERATED CRYSTALS WITH DIFFERENT REACTION TIMES

Sample	Element	Weight (%)	Atomic (%)	Uncert. (%)	Correction
15 min	Ca(K)	91.01	96.59	0.37	0.98
	Cd(K)	8.98	3.41	0.30	0.86
45 min	Ca(K)	14.88	32.89	0.31	0.98
	Cd(K)	85.12	67.10	2.19	0.86
60 min	Ca(K)	5.75	14.61	0.28	0.98
	Cd(K)	94.24	85.38	2.21	0.86
360 min	Ca(K)	1.55	4.23	0.16	0.98
	Cd(K)	98.44	95.76	2.26	0.86

To analyze the formation type of $Ca_xCd_{1-x}CO_3$ solid solution and identify whether it formed a substitutional solid solution or not, TEM-mapping measurements were performed to further investigate the above generated crystal. As illustrated in Fig. 5, C, O, Ca and Cd were regularly distributed in the crystal lattice

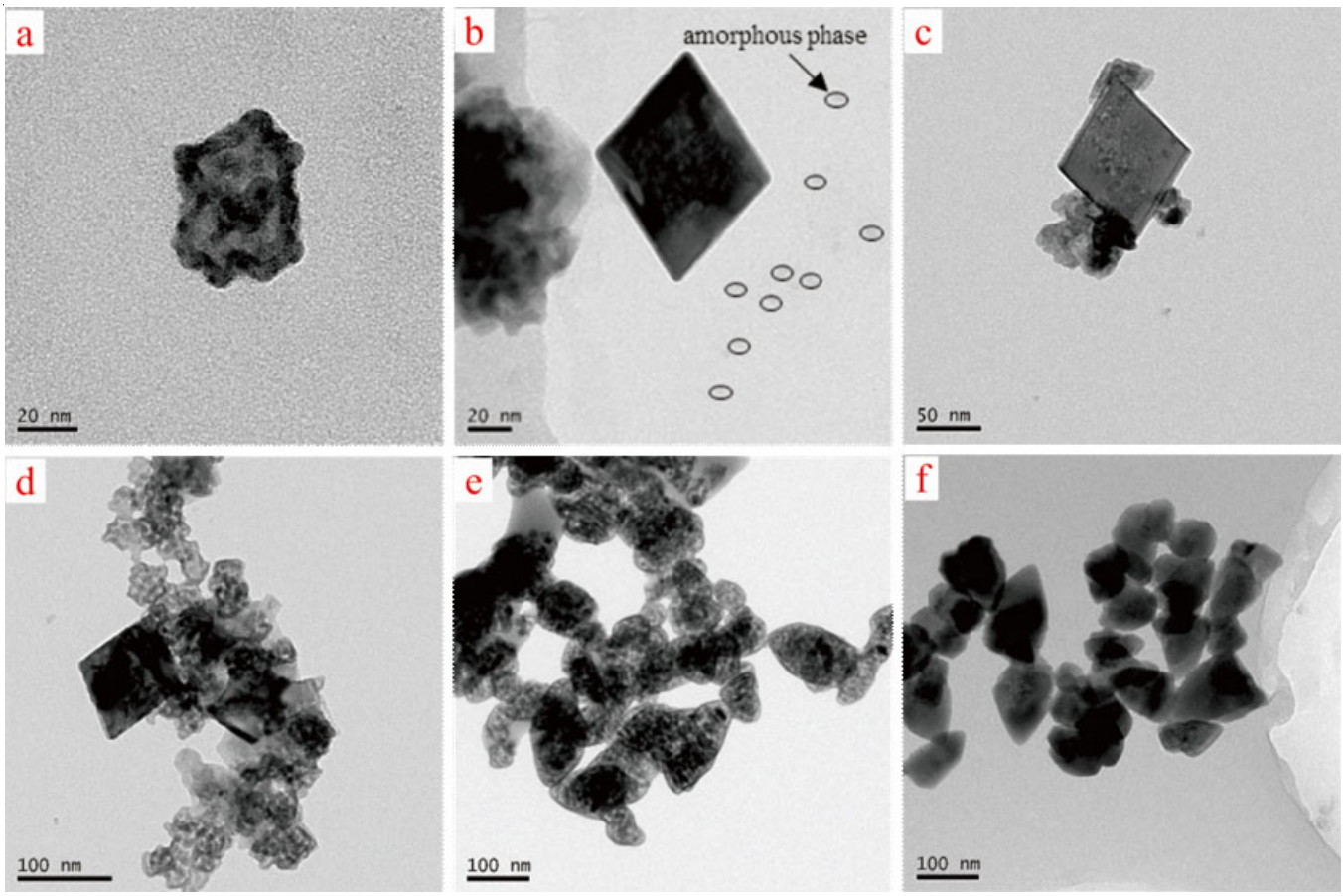

Fig. 4. TEM images of the precipitated metal carbonates after reaction for 5 min (a), 15 min (b), 30 min (c), 45 min (d), 60 min (e) and 360 min (f)

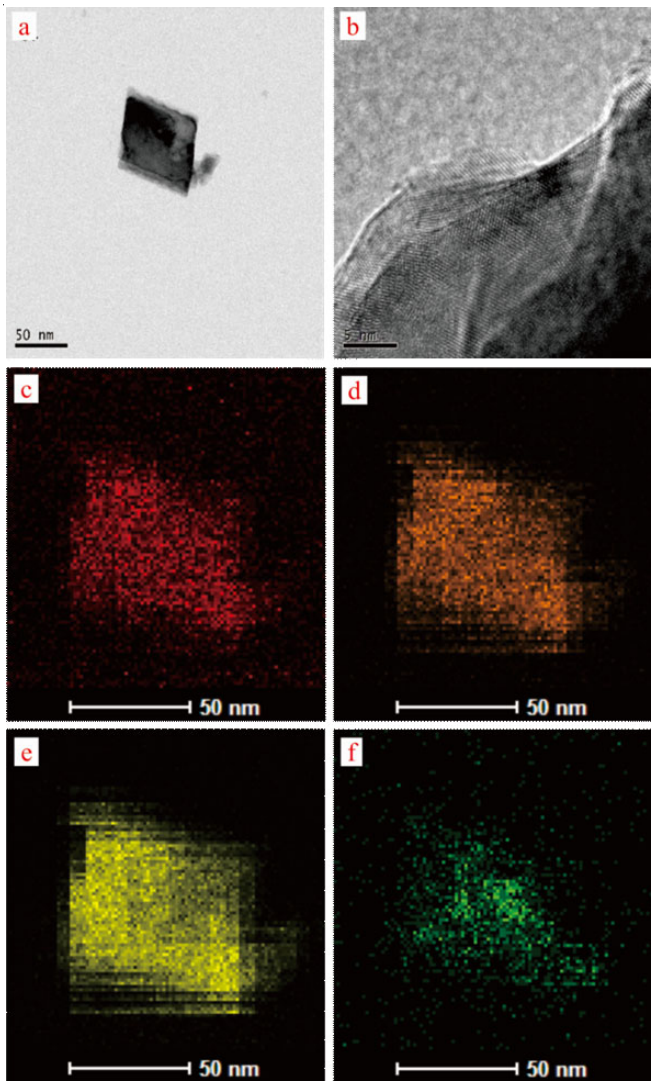

Fig. 5. HRTEM images of the existence of the $Ca_xCd_{1-x}CO_3$ solid solution (a) and high-resolution image (b). TEM-mapping results of the $Ca_xCd_{1-x}CO_3$ solid solution after reaction for 30 min: C element distribution (c), O element distribution (d), Ca element distribution (e) and Cd element distribution (f)

of generated solid solution. C and O were evenly distributed, and the distribution laws were basically the same, indicating that C and O were in the form of CO_3^{2-}. The experimental results demonstrated that generated crystal with a complete rhomboid structure was $Ca_xCd_{1-x}CO_3$ solid solution.The distribution of Ca was much higher than that of Cd atoms. This also supported the EDS experimental results from another perspective. In a short period of time, the solid solution formed was in rich Ca^{2+}. Cd^{2+} permeated into $CaCO_3$ lattice and formed a substitutional solid solution. The nanocrystal accumulated a small grain along the epitaxy of solid solution. The cadmium content of irregular flake nanocrystalline prepolymers in epitaxial aggregation was significantly higher than that in nanocrystal with a rhomboid structure. This means that the proportion of Cd atoms in the solid solution will gradually increase over time. In the upper right corner of nanocrystalline, the proportion of Ca atoms was lower than that in other regions, while the proportion of Cd atoms was higher. In a word, the new epitaxial phase had a strong tendency to concentrate cadmium.

Mechanism: The results of this experiment have sufficiently provided convincing evidence to prove the formation of $Ca_xCd_{1-x}CO_3$ solid solution and described the crystal growth process of $Ca_xCd_{1-x}CO_3$ solid solution. There are many factors influencing the growth trend and final morphology of crystals. According to thermodynamic analysis, the crystallization process depends on the balance between the solid phase and the aqueous solution. The four potential chemical reactions on calcite surface exposed to Cd-bearing aqueous solutions are described as follows:

$$CaCO_{3(s)} \Leftrightarrow Ca^{2+}(aq) + CO_3^{2-}(aq) \quad (1)$$

$$Cd^{2+}(aq) + CO_3^{2-}(aq) \Leftrightarrow CdCO_{3(s)} \quad (2)$$

$$Cd^{2+}(aq) + CaCO_{3(s)} \Leftrightarrow Ca_xCd_{1-x}CO_{3(s)} + (1-x)Ca^{2+}(aq) \quad (3)$$

$$Cd^{2+}(aq) + CaCO_{3(s)} \Leftrightarrow CdCO_{3(s)} + Ca^{2+}(aq) \quad (4)$$

Eqn. 1 represents the dissolution of calcite with the release of CO_3^{2-} to Cd-bearing aqueous solutions. Next, eqns. 2-4 may occur depending on the thermodynamics. The law of mass action for these reactions is given as follows:

$$K_{MeCO_3} = a_{Me^{2+}} a_{CO_3^{2-}} = m_{Me^{2+}} \gamma_{Me^{2+}} m_{CO_3^{2-}} \gamma_{CO_3^{2-}} \quad (5)$$

where, K_{MeCO_3} (Me = Ca, Cd) designates the equilibrium constant of reactions. a_{Me2+}, m_{Me2+} and γ_{Me2+} (Me = Ca, Cd) denote the activity, concentration and activity coefficient, respectively. In order to interpret crystal growth process with a solid solution-aqueous solution (SS-AS) system, it is necessary to evaluate the super saturation of aqueous solution with respect to the solid phases that are susceptible to precipitate, which should be used as the driving force for crystallization. The simplest one is the so-called stoichiometric super saturation (β_x). For the case of $Ca_xCd_{1-x}CO_3$–H_2O system, the stoichiometric super saturation function can be expressed as:

$$\beta_{(x)} = \frac{a(Cd^{2+})^x a(Ca^{2+})^{(1-x)} a(CO_3^{2-})}{(K_{otavite} X_{CdCO_3})(K_{calcite} X_{CaCO_3})^{(1-x)}} \quad (6)$$

where $K_{calcite}$ and $K_{otavite}$ are the solubility products of end-members of the solid solution, which are taken to be $10^{-8.48}$ and $10^{-12.1}$, respectively [20-22] and X_{CaCO_3} and X_{CdCO_3} are the molar fractions of componets $CaCO_3$ and $CdCO_3$. An explanation for that epitaxial solid solution were first rich in Ca and the Cd content increased with distance from the original calcite surface. The low-cadmium solid solution with thermodynamic instability could be transformed into a Cd-rich solid solution.

Additionally, the route of indirect production of solid solution crystals mainly includes the following steps: (a) the temporary stability of amorphous phase, (b) the transition to a stable crystal, (c) crystal selection and (d) crystal orientation. The formation of crystals requires two capabilities, namely, surface formation and crystal construction. Nucleation plays an important role in the crystallization process. The main mechanism of calcium carbonate crystallization is contact nucleation, which is produced by the crystal nucleation surface of a crystal and solid contact of the particles. The nucleation of calcium carbonate should be primarily homogeneous nucleation. According to kinetic theory, each moving element can often enter into the force field of another unit and immediately combine together. Some recent publications [23-26] have certified that the crystal orientation of the amorphous phase with a "short range order"

should be consistent with the crystalline form that was to be changed. Because the crystal lattice of otavite with lattice parameters $a_0 = 0.4923$ nm and $c_0 = 1.6287$ nm matched that of calcite with $a_0 = 0.4989$ nm and $c_0 = 1.7062$ nm, the highly oriented crystal group of carbonate solid solution could be obtained by means of epitaxy. For these reasons, $Ca_xCd_{1-x}CO_3$ solid solution has no lattice defects. Theoretical method for modeling of the incorporation of Cd into $CaCO_3$ has been the subject of numerous studies [27,28]. Significantly, together with coprecipitation, cadmium adsorption plays an important role in the interaction process.

Conclusion

The crystal growth of $Ca_xCd_{1-x}CO_3$ solid solution at 283.1 K was investigated by exposing the calcite $(10\bar{1}4)$ surface to Cd-bearing aqueous solutions and using a CO_3^{2-} diffusion method to aqueous solutions containing 0.05 M Cd^{2+} and 0.05 M Ca^{2+}. *in situ* AFM measurements were used to perform the real-time tracking of nucleation process of $Ca_xCd_{1-x}CO_3$ solid solution. SEM-EDS and TEM mapping were employed as primary techniques for the investigation of microstructure morphology and element distribution of the generated crystals. The epitaxial phase of $Ca_xCd_{1-x}CO_3$ solid solution were first rich in calcium. The content of Cd increased with distance from the original calcite surface increasing. In the process of maturation, a low-cadmium solid solution with thermodynamic instability could be transformed into a Cd-rich solid solution.The proposed mechanism of $Ca_xCd_{1-x}CO_3$ solid solution precipitation allows for early structural preformation during the pre-nucleation stage conveyed into the post-nucleation stage. The growth of these clusters is then considered to take place by the addition of single ions, and the formation of different polymorphs is considered to be under thermodynamic or kinetic control.

ACKNOWLEDGEMENTS

The authors gratefully acknowledge the financial support from National Natural Science Foundation of China (Grant No: 21607176), Natural Science Foundation of Hunan Province, China (Grant No. 2017JJ3516), Research Foundation of Education Bureau of Hunan Province, China (Grant No. 16B274), the Open fund for Key Discipline of Forestry of Central South University of Forestry and Technology (Grant No. 2016ZD11), the Science and Technology Planning Project of Hunan Province, China (No. 2016SK2088) and the Youth Scientific Research Foundation of Central South University of Forestry and Technology (104/0329).

CONFLICT OF INTEREST

The authors declare that there is no conflict of interests regarding the publication of this article.

REFERENCES

1. Y.-Y. Wang, Y.-X. Liu, H.-H. Lu, R.-Q. Yang and S.-M. Yang, *J. Solid State Chem.*, **261**, 53 (2018); https://doi.org/10.1016/j.jssc.2018.02.010.
2. H.M. Hu, X.W. Li, P.W. Huang, Q.W. Zhang and W.Y. Yuan, *J. Environ. Manage.*, **203**, 1 (2017); https://doi.org/10.1016/j.jenvman.2017.07.066.
3. Z.H. Dong, F. Zhang, D. Wang, X. Liu and J. Jin, *J. Solid State Chem.*, **224**, 88 (2015); https://doi.org/10.1016/j.jssc.2014.06.030.
4. L. Klapiszewski, K. Siwinska-Stefanska and D. Kolodynska, *Chem. Eng. J.*, **330**, 518 (2017); https://doi.org/10.1016/j.cej.2017.07.177.
5. E.B.R. Callagon, S.S. Lee, P.J. Eng, N. Laanait, N.C. Sturchio, K.L. Nagy and P. Fenter, *Geochim. Cosmochim. Acta*, **205**, 360 (2017); https://doi.org/10.1016/j.gca.2016.12.007.
6. M. Bucca, M. Dietzel, J.W. Tang, A. Leis and S.J. Köhler, *Chem. Geol.*, **266**, 143 (2009); https://doi.org/10.1016/j.chemgeo.2009.06.002.
7. C. Pérez-Garrido, L. Fernández-Díaz, C.M. Pina and M. Prieto, *Surf. Sci.*, **601**, 5499 (2007); https://doi.org/10.1016/j.susc.2007.09.021.
8. M. Prieto, A. Fernández-González, A. Putnis and L. Fernández-Díaz, *Geochim. Cosmochim. Acta*, **61**, 3383 (1997); https://doi.org/10.1016/S0016-7037(97)00160-9.
9. P.A. Rock, W.H. Casey, M.K. Mcbeath and E.M. Walling, *Geochim. Cosmochim. Acta*, **58**, 4281 (1994); https://doi.org/10.1016/0016-7037(94)90333-6.
10. Y. Du, F. Lian and L.Y. Zhu, *Environ. Pollut.*, **159**, 1763 (2011); https://doi.org/10.1016/j.envpol.2011.04.017.
11. S.L. Riechers, K.M. Rosso and S.N. Kerisit, *J. Phys. Chem. C*, **121**, 5012 (2017); https://doi.org/10.1021/acs.jpcc.6b11727.
12. P. Cubillas, S. Köhler, M. Prieto, C. Causserand and E.H. Oelkers, *Geochim. Cosmochim. Acta*, **69**, 5459 (2005); https://doi.org/10.1016/j.gca.2005.07.016.
13. J.M. Astilleros, C.M. Pina, L. Fernández-Díaz, M. Prieto and A. Putnis, *Chem. Geol.*, **225**, 322 (2006); https://doi.org/10.1016/j.chemgeo.2005.08.025.
14. M. Xu, L. Kovarik, B.W. Arey, A.R. Felmy, K.M. Rosso and S. Kerisit, *Geochim. Cosmochim. Acta*, **134**, 221 (2014); https://doi.org/10.1016/j.gca.2013.11.036.
15. M. Xu, E.S. Ilton, M.H. Engelhard, O. Qafoku, A.R. Felmy, K.M. Rosso and S. Kerisit, *Chem. Geol.*, **397**, 24 (2015); https://doi.org/10.1016/j.chemgeo.2015.01.003.
16. D. Konopacka-£yskawa, B. Koœcielska and J. Karczewski, *J. Cryst. Growth*, **478**, 102 (2017); https://doi.org/10.1016/j.jcrysgro.2017.08.033.
17. N. Wada, N. Horiuchi, M. Nakamura, K. Nozaki, T. Hiyama, A. Nagai and K. Yamashita, *J. Cryst. Growth*, **415**, 7 (2015); https://doi.org/10.1016/j.jcrysgro.2014.12.027.
18. P. Cubillas and S.R. Higgins, *Geochem. Trans.*, **10**, 7 (2009); https://doi.org/10.1186/1467-4866-10-7.
19. M.M. Reddy, *J. Cryst. Growth*, **352**, 151 (2012); https://doi.org/10.1016/j.jcrysgro.2011.12.069.
20. S.L.S. Stipp, G.A. Parks, D.K. Nordstrom and J.O. Leckie, *Geochim. Cosmochim. Acta*, **57**, 2699 (1993); https://doi.org/10.1016/0016-7037(93)90384-9.
21. B.R. Churagulov, P. Schmidt and D. Zeng, *J. Phys. Chem. Ref. Data*, **40**, 043104 (2011); https://doi.org/10.1063/1.3645087.
22. E. Königsberger, R. Hausner and H. Gamsjäger, *Geochim. Cosmochim. Acta*, **55**, 3505 (1991); https://doi.org/10.1016/0016-7037(91)90051-6.
23. H. Nada, T. Nishimura, T. Sakamoto and T. Kato, *J. Cryst. Growth*, **450**, 148 (2016); https://doi.org/10.1016/j.jcrysgro.2016.06.042.
24. P. Raiteri and J.D. Gale, *J. Am. Chem. Soc.*, **132**, 17623 (2010); https://doi.org/10.1021/ja108508k.
25. D. Gebauer, A. Volkel and H. Colfen, *Science*, **322**, 1819 (2008); https://doi.org/10.1126/science.1164271.
26. E.M. Pouget, P.H.H. Bomans, J.A.C.M. Goos, P.M. Frederik, G. de With and N.A.J.M. Sommerdijk, *Science*, **323**, 1455 (2009); https://doi.org/10.1126/science.1169434.
27. G.K. Mandell, P.A. Rock, W.H. Fink and W.H. Casey, *J. Phys. Chem. Solids*, **60**, 651 (1999); https://doi.org/10.1016/S0022-3697(98)00320-5.
28. Z.T.Y. Liu, B.P. Burton, S.V. Khare and P. Sarin, *Chem. Geol.*, **443**, 137 (2016); https://doi.org/10.1016/j.chemgeo.2016.09.024.